The thermal conductivity of plasma electrolytic oxide coatings on aluminium and magnesium

J.A. Curran, T.W. Clyne*

Department of Materials Science and Metallurgy Cambridge University, Pembroke Street, Cambridge CB2 3QZ, UK

Available online 25 February 2005

Abstract

Plasma electrolytic oxide coatings have been produced on both aluminium and magnesium substrates. Their microstructures have been studied and deductions made about formation conditions. The thermal conductivities of the coatings have been measured using a simple steady state method. The values obtained are relatively low (~1 W m^{-1} K^{-1}). This is explained in terms of the microstructure, which exhibits an extremely fine grain size and a significant proportion of amorphous phase. The porosity levels are low, so the low conductivity is not due to the presence of pores. It is noted that, even with a thickness limit of the order of 100 μm, coatings with such low conductivity may prove useful as thermal barrier layers, particularly since they exhibit excellent adhesion characteristics.
© 2005 Elsevier B.V. All rights reserved.

Keywords: Plasma electrolytic oxidation; Thermal conductivity; Amorphous; Grain structure; Nanocrystalline; Alumina coatings; Discharge channels; Microarc oxidation

1. Introduction

Plasma electrolytic oxide (PEO) coatings can be formed on a variety of alloys, with a wide range of thickness [1]. They are reported to offer attractive combinations of wear resistance [2–6] and interfacial adhesion [7,8]. The high resistance to interfacial spallation is undoubtedly due, at least in part, to strong bonding at the interface, which is formed by partial consumption of the substrate. However, it also seems likely that these coatings exhibit high strain tolerances, as a consequence of relatively low stiffness, which is caused by the presence of micro-cracks and other microstructural defects [9]. This inhibits the generation of large stresses and associated high strain energy release rates. Thus, differential thermal expansion stresses, which have been identified [1,8] as a potential source of problems for high temperature use, may in practice be unlikely to reach high levels in PEO coatings.

There has been little systematic study so far of any thermal properties of PEO coatings, although there are reports [10,11] indicating that they have good high temperature stability. In the present work, coating microstructures have been examined using X-ray diffraction and scanning electron microscopy. The thermal conductivities of thick PEO coatings were then measured, using a novel steady state method based on double-substrate specimens.

2. Experimental procedures

2.1. Sample preparation

Substrates were prepared in the form of cylinders, 30 mm in diameter and 20 mm in length, designed to fit the thermal conductivity rig (see Section 2.4). Aluminium alloy BS Al-6082 was used for study of coatings on aluminium, while AZ 91 magnesium alloy was used for study of coatings on magnesium. PEO coatings were grown on the flat end surfaces of the cylinders, using the Keronite™ process. AC power was applied with a 50 Hz modulation, applying both positive and negative potential pulses to the substrates, immersed in commercially available electrolytes. Power was controlled so as to maintain a constant current density and

* Corresponding author.
E-mail address: twc10@cam.ac.uk (T.W. Clyne).

coatings of different thickness were grown by varying the processing time. Coating thickness was measured using an Oxford Instruments CMI-100 thickness gauge, which uses eddy currents induced in the substrate to measure the coating thickness with an accuracy of about ±1 μm. The reliability of this was verified via microscopy on polished sections. Coated specimens were sectioned with a low-speed rotating diamond saw, hot-mounted in resin, ground with SiC papers and then polished using diamond paste and colloidal silica. In some cases, grinding and polishing of coating free surfaces were also used to reduce their surface roughness.

Some coatings were detached from the substrate by immersion for a minute or two in a warm, saturated solution of NaOH. These specimens were used to determine the approximate coating porosity level, using hydrostatic weighing (see Section 2.2 below).

2.2. Porosity measurement

The coating density was determined using buoyancy measurements on free-standing coatings. Coatings were weighed several times in air, to ±10 μg precision, using a Sartorius microbalance. They were then immersed in $C_{11}F_{20}$ ("Flutec") and the apparent weight re-measured. $C_{11}F_{20}$ was used primarily because of its chemical inertness and because of its wetting and penetrating abilities, but also because its high relative density helps to reduce experimental error. The difference between the two weights gives a measure of the buoyancy of the coatings.

Based on the densities of air and of the solvent, it is then possible to determine the apparent density of the coatings. Combining this with the expected value for the density of pore-free material enables an estimate of the occluded porosity to be made.

2.3. Microstructural studies

SEM observations were made using JEOL 5800 LV and JEOL 6340F FEGSEM microscopes. Some observations were made in low vacuum mode, while others were made in high vacuum on specimens sputter-coated with platinum (to minimise surface charging). X-ray diffraction was performed, using $Cu_{K\alpha}$ radiation in θ–2θ scans from $10°$ to $120°$. Data were obtained both from as-deposited free surfaces and from polished serial sections. Phase proportions were determined by Rietveld analysis [12], together with profile fitting of the low-angle amorphous peaks, and estimates of crystallite size were made from peak broadening, according to the Scherrer equation [13].

2.4. Thermal conductivity measurements

The thermal conductivity was measured, using the experimental arrangement shown in Fig. 1. Full details of the method are given elsewhere [14]. Three or four small (1 mm diameter) radial holes were drilled as far as the centreline of each cylinder. Thermocouples were then inserted to measure the temperature at these known points
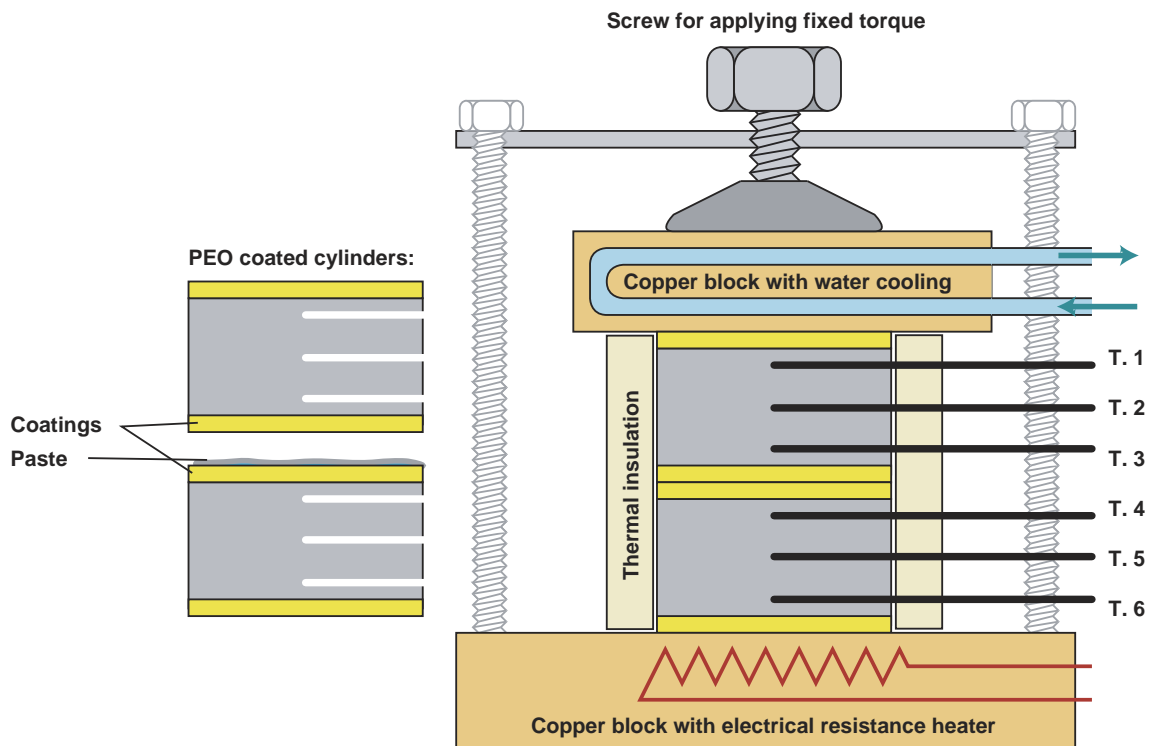

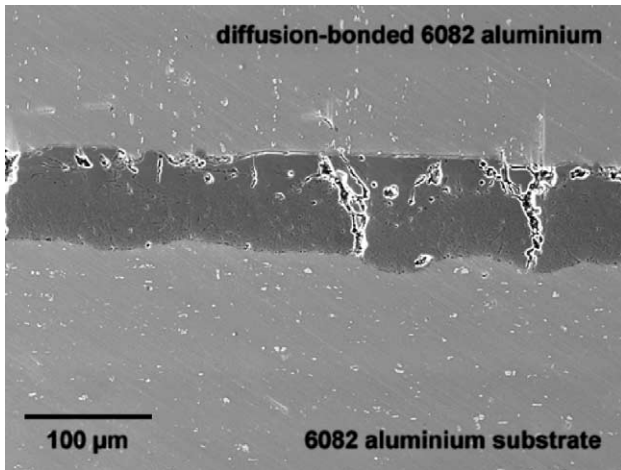Fig. 1. Experimental arrangement used for steady state measurement of thermal conductivity.

Fig. 2. SEM micrograph of a section through a coating formed on an Al alloy substrate (below), diffusion-bonded to another substrate (above), illustrating the quality of bond achieved.

along the cylinder axis. Pairs of specimens were placed in series between the heating and cooling blocks of the apparatus. A small amount (~0.1 ml) of high conductivity paste was smeared at the interfaces, and a fixed torque of 2 N m was applied to the securing screw.

Electrical resistance heating coils were then switched on (at a fixed power setting), and a steady flow of water was passed through the cooling block. Data-logging of the thermocouple output was used to determine when a steady state had been reached. Once the temperatures had been stable to within 0.5 °C for about 30 min, average thermal gradients through the blocks were established, allowing the temperature drop across the PEO coatings and hence their thermal conductivity, to be determined. The thermal conductivity of the substrate materials was measured independently, and found to be 170 W m^{-1} K^{-1} for the Al 6082 and 167 W m^{-1} K^{-1} for the AZ 91 magnesium. These values are known [15] to show little variation over the temperature range in question (50 to 200 °C).

The thermal resistance associated with the interface between the two cylinders, and its filling of "high conductivity" paste, was also taken into account. It was measured by using uncoated aluminium cylinders in the same set-up and was found to be repeatable and equivalent to a 3 ± 1 μm thickness of paste (reported conductivity 0.9 W m^{-1} K^{-1}). The paste layer therefore contributes a predictable and repeatable thermal resistance, which was subtracted from the apparent thermal resistance of the PEO coating in order to obtain the coating conductivity. As a means of providing a cross-check on the measured coating conductivity, a diffusion bonded specimen was used (Fig. 2), allowing the interface, and associated filling paste, to be eliminated. For this, it was first necessary to polish away the outermost 15–20 μm of the PEO coating. The diffusion bonding procedure used is described elsewhere [16]. A pressure of ~1 MPa was applied for a period of 1 h, at a temperature of 550 °C.

Finally, some of the measurements were repeated with the complete system located in a vacuum chamber, to assess the effect of the presence of air on the conductivity of the coatings.

3. Coating microstructure and morphology

3.1. Microstructure

Figs. 3 and 4 show back-scattered SEM micrographs of polished cross-sections of PEO coatings grown on Al 6082 and on AZ 91 magnesium, respectively. The coating on magnesium appears to be slightly more porous than that grown on the aluminium, but the overall porosity level appears to be low in both cases. However, both are characterised by the presence of extensive networks of fine-scale micro-cracks and pipe-like defects. Although the grain structure was not resolvable in the SEMs and FEGSEMs used in the present work, in the case of the alumina coatings, an estimate of the crystallite size was made from XRD peak broadening data (see Section 2.3), using high resolution X-ray diffraction data. These data suggest that the crystallite size is in the 40–80 nm size range. This is consistent with the limited TEM work published to date [4], which reported that the coating microstructure exhibited a dispersion of nano-crystalline grains (50–80 nm in diameter) in an amorphous matrix.

3.2. Phase constitution

Fig. 5 presents an X-ray diffraction spectrum for a coating grown on aluminium. The peaks correspond to a mixture of α-Al$_2$O$_3$ and γ-Al$_2$O$_3$, in roughly equal proportions. The coatings on magnesium consisted primarily of MgO (periclase) with ~6% MgAl$_3$O$_4$ spinel. Moreover, both coatings apparently contain a significant proportion of amorphous
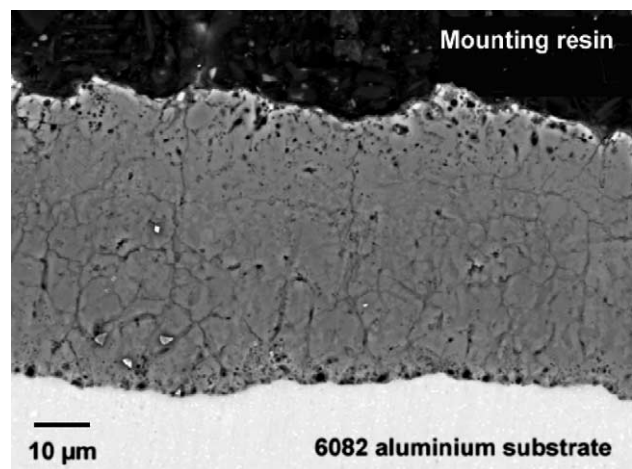

Fig. 3. Back-scattered SEM micrograph of a polished cross-section through a 100 μm thick coating on a 6082 aluminium substrate.
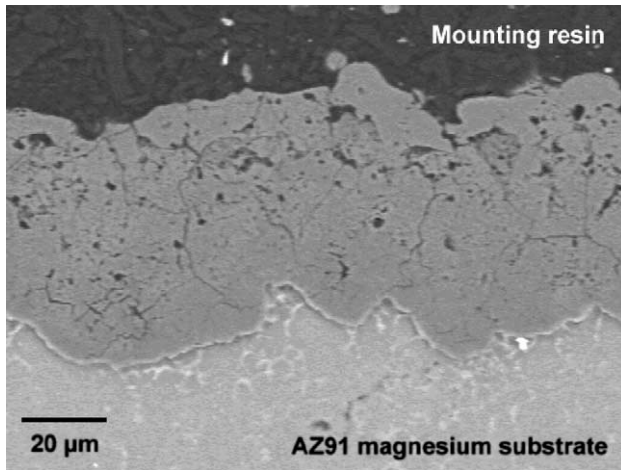
Fig. 4. Back-scattered SEM micrograph of a polished cross-section through a 60 μm thick coating on a AZ91 magnesium alloy substrate.

material, as indicated by a broad peak in the background signal (see Fig. 5, in 2θ range of ~$30°$–$40°$). For both Al- and Mg-based coatings, the amorphous content has been estimated at around 30%. Previous work by the present authors [9] has shown this amorphous constituent to be fairly uniformly distributed throughout the thickness of the coatings. This amorphous material, like the metastable γ-Al_2O_3, is believed to form during rapid localised quenching, which occurs around each individual discharge during the formation process. The presence of such amorphous material is expected to have a significant effect on the thermal conductivity of the coatings—see Section 4.1.

3.3. Porosity levels

The density of the alumina coatings was measured as 3.61 ($\pm$0.03) g cm^{-3}. Taking the expected average density of fully dense α-Al_2O_3 to be 3.98 $\pm$0.02 g cm^{-3}, γ-Al_2O_3 to be 3.7 ($\pm$0.2) g cm^{-3}, and (anodically grown) amorphous alumina [17] to be 3.10 ($\pm$0.05) g cm^{-3}, and using the relative proportions described in Section 3.2, the deduced density of the PEO alumina coating is 3.6 ($\pm$0.2) g cm^{-3}. This suggests that the fraction of occluded porosity is very small (<~1%), although the uncertainty in the estimated density of fully dense material is such that the upper bound is probably about 3–4%. This is clearly a very approximate exercise, and some of the porosity present may be surface-connected, but it may nevertheless be concluded that the porosity levels in these coatings must be relatively low. This is broadly consistent with the microstructural appearance (Figs. 2 and 3) which appears to confirm that the porosity levels are less than 5%. Such levels of porosity, if dispersed fairly uniformly, would not be expected to have any substantial effect on the thermal conductivity of the coatings. Furthermore, the difference between conductivities measured in air and in vacuum would be expected to be small.

4. Thermal conductivity

4.1. A simple analytical prediction

A prediction can be made of the thermal conductivity of these coatings, based on the grain size and the proportion of amorphous material present, together with values of the conductivity of single crystal and amorphous material. This assumes a distribution of grains in an amorphous matrix, such that an inverse rule of mixtures is appropriate for estimation of the effective conductivity. It is clearly a gross simplification, with no account taken of phonon scattering or mean free path effects.
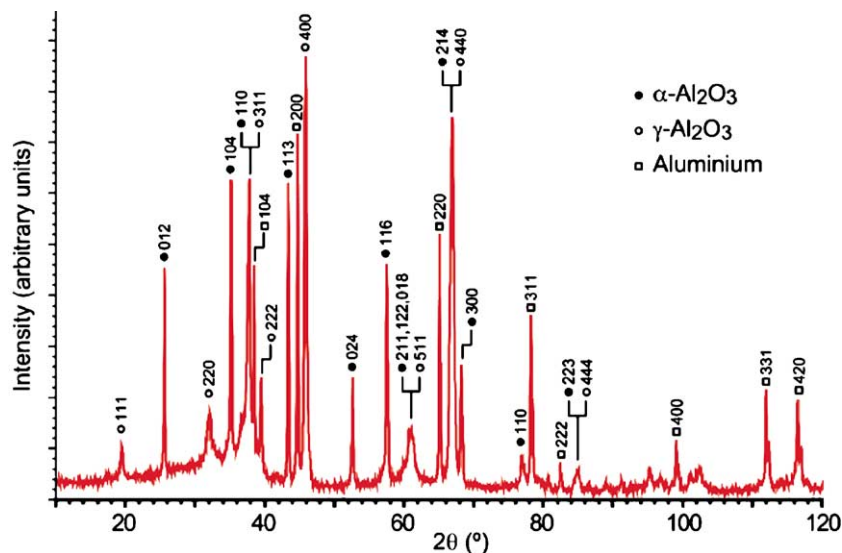

Fig. 5. Typical X-ray diffraction spectrum, from $2\theta=10°$ to $120°$ for a coating grown on aluminium 6082.

For a grain size, d, and a volume fraction of amorphous material, f_a, the amorphous material may be considered as a grain boundary of thickness t where:

$$t = \frac{f_a d}{1 - f_a} \qquad (1)$$

If the thermal conductivities of the grain, K_{sc}, and the grain boundary (amorphous) material, K_a, are known, then the effective thermal conductivity of the overall path (of length $t+d$) may be calculated from the sum of thermal resistivities:

$$K_{eff} = \frac{t + d}{\dfrac{t}{K_a} + \dfrac{d}{K_{sc}}} \qquad (2)$$

The measurements of Smith et al. [18] on alumina refractories established the thermal resistance of a grain boundary to be about 1.3×10^{-8} m^2 W^{-1} K. It follows that the thermal conductivity of amorphous alumina (assumed to have a structure similar to that within a typical grain boundary, which has an effective thickness of the order of 1 nm) is ~0.1 W m^{-1} K^{-1} (it is, of course, expected that amorphous ceramics will exhibit a much lower thermal conductivity than crystalline phases with a similar chemical composition, since phonon scattering is much greater in disordered structures). The thermal conductivity can thus be predicted as a function of grain size, using Eq. (2), and the result of such a calculation is shown in Fig. 6.

Assuming crystallites in the 40–80 nm size range (Section 3.1), this suggests that the thermal conductivity of these coatings might be expected to be as low as 0.2–0.8 W m^{-1} K^{-1}. This is broadly consistent with the fact that anodically-grown alumina films typically exhibit thermal conductivities up to an order of magnitude lower than the bulk value for the ceramic [18,19].

4.2. Discussion of results

For the *aluminium* alloy specimens, a typical temperature profile in the steady state exhibited a temperature
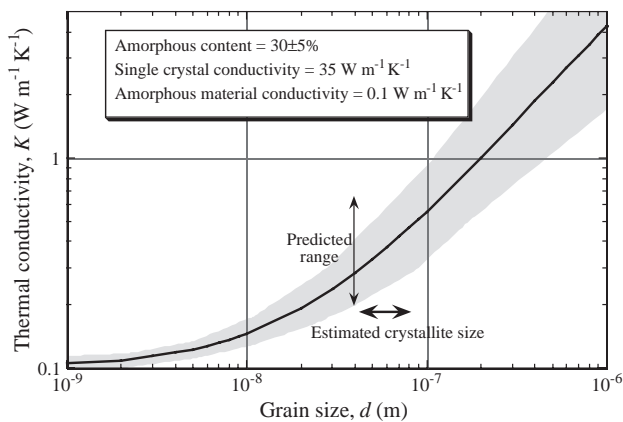

Fig. 6. Predicted thermal conductivity as a function of grain size, obtained using Eq. (2), with the range of experimentally-determined crystallite sizes indicated on the plot.
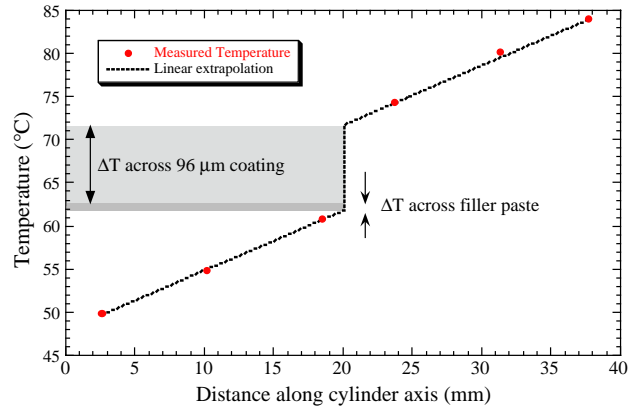

Fig. 7. A typical steady state thermal profile for coated aluminium.

drop across the sample of about 100 °C, with a 10 °C temperature difference developing across the coating (100 μm thick)—see Fig. 7. Thermocouple data are considered to be accurate to within 0.5 °C, and their locations are known to within about 0.5 mm. There is also a significant uncertainty in the value of the coating thickness. Such profiles indicate that (after subtracting the contribution from the interfacial filler paste) the thermal conductivity of the coating is about 1.6 ± 0.4 W m^{-1} K^{-1}. While this figure cannot be regarded as very accurate, it is clearly about an order of magnitude lower than typical values reported [20] for single crystal Al$_2$O$_3$ (32–34 W m^{-1} K^{-1}). This effect cannot be accounted for by porosity alone, since even levels of around 5% (Section 3.3), if uniformly dispersed, would not be expected to induce a reduction of more than about 5–10%. However, the measured value is broadly consistent with the range predicted using the simple model presented for the effect of the amorphous content (Section 4.1).

The value obtained for the diffusion-bonded specimen was 1.8 W m^{-1} K^{-1}, which is not significantly different, suggesting that the procedure for evaluating the interface resistance due to filler paste is acceptable. Results obtained using coatings of various thickness (from 40 to 100 μm) did not indicate any dependence of the
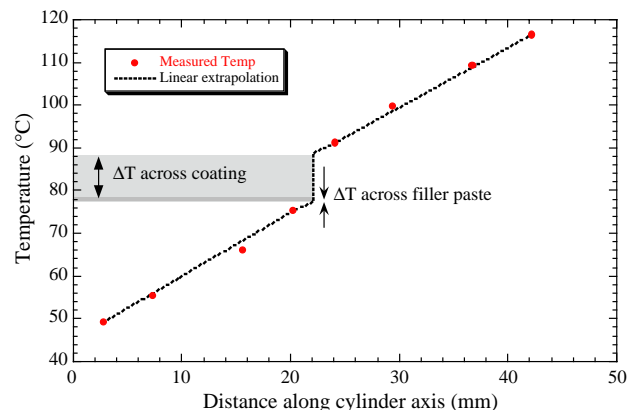

Fig. 8. A typical steady state thermal profile for coated magnesium.

conductivity on coating thickness. Prior polishing (removing as much as 30% of the coating thickness) also had no noticeable effect on the measured conductivity. These results are consistent with the assumption of approximately uniformly distributed porosity made in Section 3.3, but really just underline the insignificance of the porosity, as far as thermal conductivity is concerned.

Measurements performed in vacuum gave a value of 1.8 ± 0.3 W m^{-1} K^{-1}, which is again not significantly different. This is yet again consistent with the observation that porosity plays no significant role in determining the thermal conductivity. This is also relevant to prediction of the effective conductivity of such coatings in high-pressure environments. In the case of plasma-sprayed zirconia coatings, used as thermal barrier coatings in gas turbines, it is thought [21] that the presence of high-pressure gas in the pores may significantly raise the thermal conductivity. Coatings which do not depend on the presence of porosity for their low thermal conductivity would not exhibit any such increase.

For the *magnesium* alloy specimens (see Fig. 8), the measured thermal conductivity was 0.8 (± 0.3) W m^{-1} K^{-1}. It again appears likely that the fine (partially amorphous) microstructure of the coatings is responsible for the greatly reduced conductivity, compared with typical values for bulk periclase or spinel (46.2 W m^{-1} K^{-1} and 11.8 W m^{-1} K^{-1}, respectively [20]). It seems likely that this is a general effect, resulting from the conditions of PEO coating growth. It can be accounted for by the fine grain size and the amorphous content, which form as a consequence of the very rapid solidification occurring during PEO formation.

The fact that measured thermal conductivities are low, despite the absence of substantial porosity, means that these coatings may have the potential to offer stable thermal protection. This low conductivity is expected to be more resistant to change during prolonged exposure to high temperatures than highly porous materials, which often undergo sintering at high temperature. Grain growth or devitrification processes might be expected to induce increases in the conductivity of PEO coatings, but in practice these are unlikely to be significant, since these coatings cannot be exposed to temperatures above about $0.4T_\mathrm{f}$ (where T_f is the absolute melting temperature of the ceramic) without the substrate melting.

5. Summary

The following conclusions can be drawn from this work.

(i) PEO coatings on both aluminium and magnesium contain about 30% amorphous material, together with fine nanocrystalline grains.

(ii) Measured thermal conductivities of PEO coatings have been found to be at least an order of magnitude
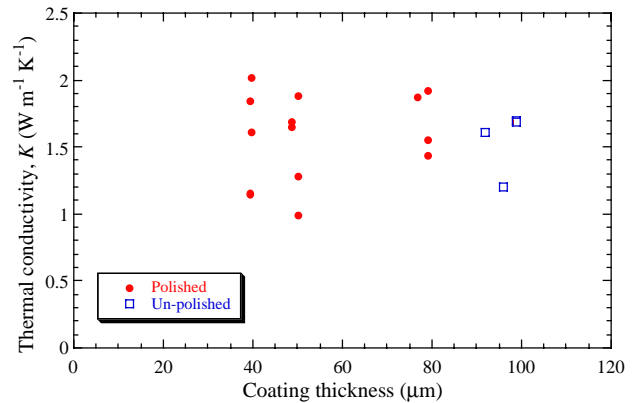

Fig. 9. Summary of thermal conductivity data for coatings on aluminium, including both polished and unpolished coatings.

lower than typical values for corresponding bulk material. For coatings on Al and Mg, measured values are 1.6 (± 0.4) W m^{-1} K^{-1} (Fig. 9) and 0.8 (± 0.3) W m^{-1} K^{-1}, respectively, which may be compared with corresponding expected bulk values of ~30 W m^{-1} K^{-1} and ~20 W m^{-1} K^{-1}.

(iii) The relatively low thermal conductivity of PEO coatings is thought to be due primarily to the presence of a high proportion of amorphous material, together with a fine grain size. A simple model has been used to confirm that this is at least a plausible hypothesis.

(v) Measured conductivities do not show any significant dependence on the presence or absence of a gaseous atmosphere. This is consistent with the observation that the porosity levels in these coatings are relatively low ($<$~5%). It might thus be expected that relatively low conductivities would be retained even in high pressure environments.

(vi) Since the amorphous and nanocrystalline structure of PEO coatings appears to be a consequence of the mechanism of formation, it is likely that the effect will be reproduced in other PEO coatings, which are thus expected to have similarly low thermal conductivities.

References

[1] A.L. Yerokhin, X. Nie, A. Leyland, A. Matthews, S.J. Dowey, Surf. Coat. Technol. 122 (1999) 73.

[2] A.A. Voevodin, A.L. Yerokhin, V.V. Lyubimov, M.S. Donley, J.S. Zabinski, Surf. Coat. Technol. 86-7 (1996) 516.

[3] J. Tian, Z.Z. Luo, S.K. Qi, X.J. Sun, Surf. Coat. Technol. 154 (2002) 1.

[4] X. Nie, E.I. Meletis, J.C. Jiang, A. Leyland, A.L. Yerokhin, A. Matthews, Surf. Coat. Technol. 149 (2002) 245.

[5] L.R. Krishna, K.R.C. Somaraju, G. Sundararajan, Surf. Coat. Technol. 163–164 (2003) 484.

[6] R. Barik, J.A. Wharton, R.J.K. Wood, K.R. Stokes, R.L. Jones, in: J. Sedriks, V. Agarwala, R. Mantz, J. Beatty (Eds.), Tri-service Corrosion Conference, (November) 2003, Navmar Applied Science Corp., Chester, PA, Las Vegas.

[7] X. Nie, A. Leyland, H.W. Song, A.L. Yerokhin, S.J. Dowey, A. Matthews, Surf. Coat. Technol. 119 (1999) 1055.

[8] S.V. Gnedenkov, O.A. Khrisanfova, A.G. Zavidnaya, S.L. Sinebru-khov, P.S. Gordienko, S. Iwatsubo, A. Matsui, Surf. Coat. Technol. 145 (2001) 146.

[9] J.A. Curran, T.W. Clyne., Surf. and Coat. Techn. (this issue).

[10] P.I. Butyagin, Y.V. Khokhryakov, A.I. Mamaev, Mater. Lett. 57 (2003) 1748.

[11] S.V. Gnedenkov, O.A. Khrisanfova, A.G. Zavidnaya, S.L. Sinebru-khov, A.N. Kovryanov, T.M. Scorobogatova, P.S. Gordienko, Surf. Coat. Technol. 123 (2000) 24.

[12] D.B. Wiles, R.A. Young, J. Appl. Crystallogr. 14 (1981) 149.

[13] R.L. Snyder, J. Fiala, H. Bunge, Defect and microstructural analysis by diffraction, Oxford University Press, 1999.

[14] J.C. Tan, I.O. Golosnoy, S.A. Tsipas, J.A. Curran, T.W. Clyne, J. Mat. Sci. (submitted for publication).

[15] F.P. Incropera, D.P. Dewitz, Fundamentals of heat and mass transfer, John Wiley, 2002.

[16] A.A. Shirzadi, E.R. Wallach, Surface Treatment of Oxidizing Materials, US Patent 6669534, 2003.

[17] G. Alcala, P. Skeldon, G.E. Thompson, A.B. Mann, H. Habazaki, K. Shimizu, Nanotechnology 13 (2002) 451.

[18] D.S. Smith, S. Fayette, S. Grandjean, C. Martin, J. Am. Ceram. Soc. 86 (2003) 105.

[19] K. An, K.S. Ravichandran, R.E. Dutton, S.L. Semiatin, J. Am. Ceram. Soc. 82 (1999) 399.

[20] R.E. Bolz, G.L. Tune, Handbook of tables for applied engineering science, CRC Press, Cleveland, OH, 1973.

[21] I.O. Golosnoy, S.A. Tsipas, T.W. Clyne, J. Therm. Spray Technol. (in press).